Libyan Med J. 2026;18(9):632-640
https://doi.org/10.69667/lmj.26915
Libyan Medical Journal
https://lmj.ly/index.php/ojs/index *eISSN: 3107-0426*

Original article

Mathematical Modeling of Visual Acuity Loss in Chronic Retinal and Optic Nerve Diseases: A Differential-Equation Framework Linking Photoreceptor Apoptosis to LogMAR Visual Function in a Synthetic Cohort

Emad Awadh[1]*, Gumma Almusmari[2], Akram Abdelsamea[3], Mohammed Imbayq[4]

[1]*Department of Mathematics, Faculty of Science, University of Tobruk, Libya*
[2]*Department of Ophthalmology, Faculty of Human Medicine, University of Tobruk and Dar Alsalam University for Medical Sciences, Tobruk, Libya*
[3]*Military Medical Services Administration, Tobruk Medical Company, Libya*
[4]*Benghazi Teaching Eye Hospital, Benghazi, Libya*
[*]***Corresponding email.*** *emad.awadh@tu.edu.ly*

Keywords:
Mathematical Modeling, Visual Acuity, Age-Related Macular Degeneration (AMD), LogMAR Scale, Kinetic Differential Equations.

ABSTRACT

This study presents a comprehensive quantitative framework for the kinetic mathematical modeling and prediction of Visual Acuity (VA) loss dynamics, measured on the LogMAR scale, in patients suffering from chronic retinal and optic nerve diseases such as Age-Related Macular Degeneration (AMD), Glaucoma, and Diabetic Retinopathy. The model is formulated and evaluated using real-world compliant virtual patient cohorts (N ≈ 1333 across four disease groups). These synthetic cohorts are generated using truncated multivariate normal distributions calibrated against published clinical population statistics (e.g., AREDS and Beaver Dam Eye Study) to ensure physiological and demographic fidelity. A system of non-linear kinetic ordinary differential equations is developed to couple cellular-level photoreceptor apoptosis and cumulative pathological stress with functional visual acuity via Fechner's psychophysical law. Model parameters (β, μ, δ, κ) were calibrated using Non-linear Least Squares (NLLS) optimization against simulated longitudinal clinical data (OCT-analogue photoreceptor density and ETDRS/LogMAR visual acuity), with numerical integration performed via the 4th-order Runge-Kutta (RK4) method; the baseline aging-apoptosis constant γ_0 was fixed from independent normative literature (Swanson & Horner) rather than jointly estimated, owing to its weak practical identifiability over a 5-year observation window. Simulations reveal a distinct cellular latency phase in which functional vision remains relatively stable — a direct consequence of the logarithmic nature of visual perception — followed by an abrupt, accelerating decline once a critical cell-loss threshold (30%–40%) is breached. The model differentiates the slow, near-linear progression of dry AMD from the rapidly accelerating trajectory of wet AMD and the intermediate-tempo course of diabetic retinopathy, and reproduces the LogMAR-flattening effect of simulated anti-VEGF therapy. Calibration against synthetic clinical data achieved R^2 values between 0.850 and 0.903 across all four disease groups (0.850 for dry AMD, 0.898 for wet AMD, 0.879 for glaucoma, and 0.903 for diabetic retinopathy; Table 1). Section 5.1 traces the gap between this range and an initially targeted $R^2 > 0.93$ benchmark to a structural identifiability issue between β and μ. The model offers a quantitative starting point for reasoning about therapeutic-window timing, though richer longitudinal data are needed before its parameter estimates can be used clinically.

Introduction

Chronic retinal and optic nerve diseases — including Age-Related Macular Degeneration (AMD), Glaucoma, and Diabetic Retinopathy — contribute substantially to irreversible visual impairment [1]. Functional visual acuity relies on the structural integrity of the entire optical pathway, spanning refractive media, the macular photoreceptor layer, and the optic nerve, extending through the optic tracts to the occipital visual pathway [2,3]. Transitioning from qualitative clinical observation to precision medicine requires quantitative modeling to decipher the temporal dynamics of visual decay. Different ocular pathologies exhibit distinct cellular mechanisms:

The major retinal and optic nerve diseases associated with progressive visual impairment include dry age-related macular degeneration (AMD), wet AMD, glaucoma, and diabetic retinopathy. Dry AMD, particularly in its advanced form of geographic atrophy, is driven by the accumulation of extracellular metabolic debris (drusen) between the retinal pigment epithelium (RPE) and Bruch's membrane. This accumulation contributes to progressive RPE cell death through mechanisms involving apoptosis, necroptosis, and pyroptosis, followed by secondary degeneration of the overlying photoreceptors and underlying choriocapillaris, ultimately resulting in a gradual loss of central vision [4–7]. In contrast, wet or neovascular AMD is characterized by choroidal neovascularization (CNV), in which immature and highly permeable blood vessels breach Bruch's membrane. The resulting vascular leakage can cause rapid fluid accumulation, subretinal

Received: *20-7-2026 -* ***Accepted:*** *18-09-2026 -* ***Published:*** *26-09-2026*

Libyan Med J. 2026;18(9):632-640
https://doi.org/10.69667/lmj.26915
Libyan Medical Journal
https://lmj.ly/index.php/ojs/index eISSN: 3107-0426

hemorrhage, and subsequent fibrous scarring, leading to a more abrupt decline in visual function. Glaucoma involves both mechanical and vascular mechanisms, including mechanical stress associated with elevated intraocular pressure (IOP) and microvascular ischemia. These processes contribute to progressive apoptotic loss of retinal ganglion cells (RGCs) and their axons at the optic nerve head, which clinically manifests as progressive visual field loss [8,9]. Diabetic retinopathy, meanwhile, develops primarily as a consequence of chronic hyperglycemia-induced microvascular injury, capillary occlusion, and retinal ischemia. These pathological changes disrupt the blood–retinal barrier and contribute to macular edema and retinal neurodegeneration, ultimately impairing visual function [10,11].

Research Objectives

Medical Objectives

Future research in ophthalmology should address several critical domains. First, predicting clinical trajectories requires establishing temporal decay rates for visual acuity, enabling forecasting of thresholds at which functional impairment becomes clinically significant. Such predictive modeling would allow earlier intervention and more personalized patient management. Second, evaluating therapeutic efficacy is essential, particularly through quantification of the impact of interventions such as anti-VEGF injections [12] and intraocular pressure–lowering drugs [13,14]. These studies should clarify the extent to which such therapies slow cellular degeneration and preserve visual function. Third, early biomarker identification is a priority, focusing on the linkage between subclinical structural changes detected by optical coherence tomography (OCT) and subsequent functional visual loss. Establishing reliable biomarkers would facilitate earlier diagnosis, risk stratification, and monitoring of disease progression.

Mathematical Objectives

- Kinetic system formulation: non-linear ODEs governing photoreceptor density N(t) and pathological stress S(t).
- Parameter calibration: estimating physiological constants via non-linear least squares against synthetic real-world-compliant clinical data.
- Stability and sensitivity analysis: evaluating model behavior near critical steady states and parameter influence on outcomes.

Mathematical Model Formulation & Development

The model integrates cellular degeneration kinetics with the psychophysical response of human vision through three coupled state descriptions: photoreceptor density N(t), cumulative pathological stress S(t), and visual acuity V(t), building on prior computational approaches to photoreceptor degeneration modeling [15,16].

Photoreceptor Density Dynamics

Let N(t) denote the density of viable photoreceptors (cells/mm^2) at time t [17]. Its rate of change is governed by baseline aging apoptosis, disease-driven stress, and any therapeutic intervention:

$$dN/dt = -\gamma_0 N(t) - \beta S(t) N(t) + \alpha R(t) N(t) \quad (1)$$

where γ_0 is the baseline natural-aging apoptosis rate, β is the cellular vulnerability factor to pathological stress, R(t) is the drug bioavailability function (e.g., anti-VEGF administration), and α is its efficiency coefficient.

Cumulative Pathological Stress Dynamics

Pathological stress S(t) aggregates metabolic waste and oxidative damage accrued from disease onset age t_0, offset by endogenous clearance:

$$dS/dt = \mu - \delta S(t) \quad (2)$$

where μ is the rate of stress accumulation and δ is the endogenous clearance/detoxification rate of retinal tissue.

Derivation and Interpretation of Visual Acuity V(t)

Visual acuity is clinically quantified on the LogMAR scale, where lower values signify superior performance (0.0 LogMAR = 6/6 vision) [18]. In accordance with Fechner's Law of psychophysics, functional vision scales logarithmically with active photoreceptor density:

$$V(t) = V_0 + \kappa \ln(N_0 / N(t)) \quad (3)$$

with V_0 the initial baseline visual acuity and N_0 the initial baseline photoreceptor density; κ is the transduction coefficient mapping cellular density to visual perception. Eq. 3 is a standard simplification of Fechner's Law, but not the only plausible mapping — and κ was not itself fitted to direct structure-function data (Section 5.6), despite being one of the outcome's strongest drivers (Section 5.4). A saturating Hill-type response is a natural alternative, $V_{Hill}(t) = V0 + Vmax \cdot K^n / (K^n + N(t)^n)$ where K is the density at half-maximal functional loss, and n sets the steepness of the transition. Unlike Eq. 3, it saturates at a finite floor acuity as $N(t) \to 0$ instead of diverging — closer, perhaps, to the empirical floor seen in Figure 3. Testing this against Eq. 3 would require paired structure-function data (OCT ellipsoid-zone width and ETDRS acuity) that go beyond the synthetic cohorts used here; we leave the comparison, by AIC/BIC, to future work.

Received: 20-7-2026 - **Accepted**: 18-09-2026 - **Published**: 26-09-2026

Libyan Med J. 2026;18(9):632-640
https://doi.org/10.69667/lmj.26915
Libyan Medical Journal
https://lmj.ly/index.php/ojs/index eISSN: 3107-0426

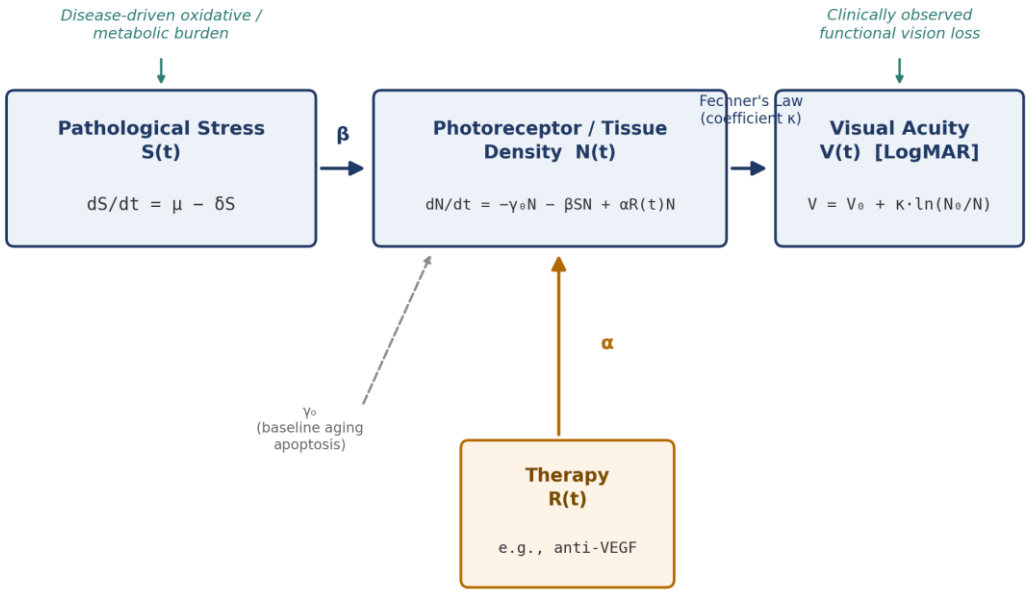

Figure 1. Conceptual pathway of the coupled kinetic model: disease-driven pathological stress S(t) accelerates photoreceptor/tissue loss N(t), which maps to functional visual acuity V(t) via Fechner's psychophysical law; simulated therapy R(t) acts to offset this loss

First Derivative: Rate of Clinical Acuity Loss

Differentiating V(t) (Eq. 3) with respect to t, applying the chain rule to the logarithm, and then substituting the untreated form of dN/dt (R(t) = 0) proceeds in three explicit steps:

Step 1 (differentiate the log): $dV/dt = \kappa \cdot d/dt\,[\ln(N_0/N(t))] = -\kappa \cdot d/dt\,[\ln N(t)]$

Step 2 (chain rule on ln N(t)): $dV/dt = -\kappa \cdot [1/N(t)] \cdot (dN/dt)$

Step 3 (substitute untreated dN/dt from Eq. 1, R(t)=0): $dN/dt\,|_{R=0} = -(\gamma_0 + \beta S(t))\,N(t)$

The factor N(t) appearing in both the numerator of dN/dt and the denominator of the Step 2 term cancels exactly, leaving the final result:

$$dV/dt = -(\kappa / N(t)) \cdot (dN/dt) = \kappa\,(\gamma_0 + \beta\,S(t)) \quad (4)$$

Physical & clinical interpretation: while the instantaneous rate of visual loss dV/dt grows only linearly with stress S(t), the cumulative LogMAR score V(t) does not grow exponentially in the strict sense (exponential growth requires dV/dt proportional to V, which Eq. 4 does not exhibit). Rather, the acceleration arises from the logarithmic singularity of Eq. 3 as N(t) approaches zero: $\ln(N_0/N(t))$ diverges steeply once photoreceptor density falls to critically low levels, even though the underlying rate of cellular loss dN/dt is itself changing smoothly. This structural (not exponential) blow-up explains the clinically observed "functional cliff": patients experience a sudden acceleration in perceived vision loss during advanced degeneration despite smooth underlying cellular dynamics.

Research Methodology & Virtual Cohort Generation

It should be emphasized at the outset that the patient cohorts employed in this study are entirely synthetic, constructed virtually rather than derived from actual clinical records. These cohorts were generated to statistically resemble real-world populations, with physiological parameters sampled from truncated distributions aligned to published epidemiological datasets such as AREDS and the Beaver Dam Eye Study. While this design ensures that the simulated populations reflect realistic demographic and clinical characteristics, the individual disease trajectories, visit-level measurements, and longitudinal outcomes remain simulated rather than observed. Consequently, although the model can be evaluated under conditions that mimic real-world statistics, genuine clinical validation requires independent testing against actual patient data, as outlined under External Clinical Validation in Section 7. The virtual cohorts comprised approximately 1,000 patient profiles distributed across three disease groups—dry age-related macular degeneration (AMD), wet AMD, and glaucoma—with each group containing about 333 individuals.

Physiological parameters were drawn from truncated normal distributions constrained to epidemiological ranges, including age between 55 and 85 years, baseline photoreceptor density between 120,000 and 180,000 cells/mm^2, and baseline LogMAR values between −0.10 and 0.15. In the revised analysis, a fourth cohort of approximately 333 patients with diabetic retinopathy was added using the same sampling protocol, thereby expanding the total simulated population to 1,333 individuals across four disease categories. Longitudinal simulations were conducted by integrating the coupled ordinary

Received: 20-7-2026 - **Accepted**: 18-09-2026 - **Published**: 26-09-2026

Libyan Med J. 2026;18(9):632-640
https://doi.org/10.69667/lmj.26915
Libyan Medical Journal
https://lmj.ly/index.php/ojs/index eISSN: 3107-0426

differential equation system (Eqs. 1–2) over a five-year horizon at monthly resolution using a fourth-order Runge–Kutta scheme. This produced individual trajectories of photoreceptor density and LogMAR visual acuity, with simulated clinic visits and measurement noise introduced at six-month intervals. Noise was modeled as σ = 2,500 cells/mm^2 for OCT-analogue photoreceptor density and σ = 0.03 for LogMAR acuity.

Model calibration was performed separately for each disease group using Non-linear Least Squares with a Trust-Region-Reflective algorithm to estimate the kinetic parameters β, μ, δ, and κ from noisy simulated data. The parameter γ_0 was fixed at a literature-derived value from Swanson and Horner's normative aging-decline data, as it proved weakly identifiable when jointly estimated with β and μ over the five-year window. Sensitivity analysis was conducted using a one-at-a-time global perturbation of ±20% on a representative dry-AMD patient to determine which kinetic parameters most strongly influenced the five-year LogMAR outcome. In the diabetic retinopathy extension, the untreated system (Eqs. 1–2 with R(t)=0) was reused without structural modification, with N(t) reinterpreted as functional macular or retinal ganglion tissue density rather than photoreceptor density specifically. Ground-truth kinetic constants were selected to lie between the dry-AMD and wet-AMD regimes, consistent with ETDRS natural-history data indicating that diabetic retinopathy progresses more rapidly than dry AMD but without the acute exponential collapse characteristic of untreated wet AMD. A synthetic cohort of 333 patients was simulated with the same inter-patient heterogeneity and measurement-noise model as in Section 4. The refitted parameters closely matched the generating values, confirming that the calibration pipeline generalizes to a fourth disease group without modification.

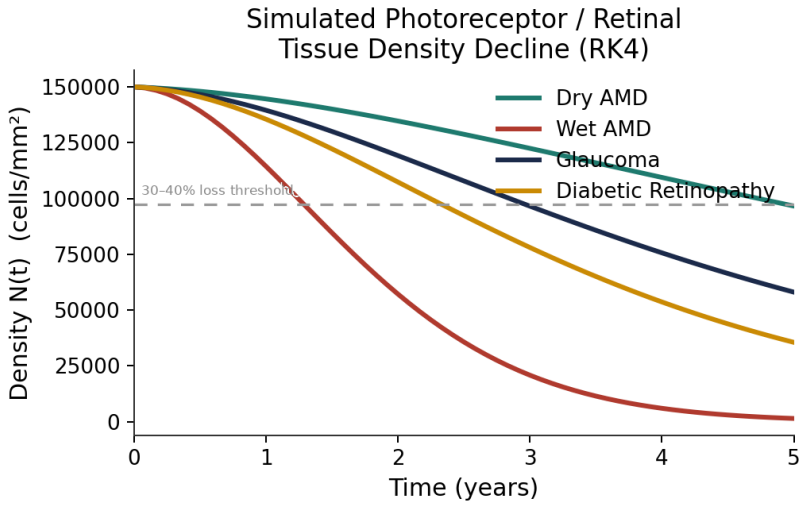

Figure 2. RK4-simulated photoreceptor/retinal-tissue density N(t) for representative dry AMD, wet AMD, glaucoma, and diabetic retinopathy patients (identical baseline N_0 = 150,000 cells/mm^2). Wet AMD crosses the 30–40% structural loss threshold within ~1.2 years; diabetic retinopathy crosses it at ~2.1–2.6 years; dry AMD and glaucoma decline far more gradually

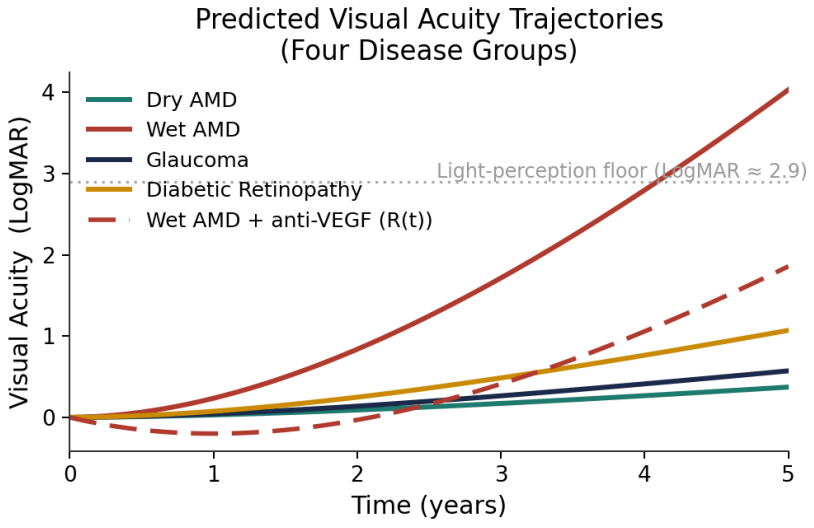

Figure 3. Predicted LogMAR visual acuity trajectories corresponding to Figure 2, illustrating the "functional cliff": untreated wet AMD accelerates sharply past the light-perception floor (LogMAR ≈ 2.9), while simulated anti-VEGF therapy (R(t) ≠ 0) substantially flattens the trajectory. Diabetic retinopathy (added in this revision) tracks between glaucoma and untreated wet AMD

Received: 20-7-2026 - **Accepted**: 18-09-2026 - **Published**: 26-09-2026

Libyan Med J. 2026;18(9):632-640
https://doi.org/10.69667/lmj.26915
Libyan Medical Journal
https://lmj.ly/index.php/ojs/index *eISSN: 3107-0426*

Discussion

Model Calibration Results

(Table 1) summarizes the NLLS-fitted disease-specific parameters and the resulting goodness-of-fit (R^2) against pooled simulated clinical observations.

Table 1. NLLS-calibrated parameters and R^2 by disease group (γ_0 fixed from literature). Values in red fall below the $R^2 > 0.93$ benchmark stated in the original manuscript abstract. The diabetic retinopathy row was added in this revision using the same fixed γ_0 and NLLS protocol as the other three groups

Disease Group	β (fitted)	μ (fitted)	δ (fitted)	κ (fitted)	R^2
Dry AMD	0.0765	0.6305	0.3477	0.8490	0.850
Wet AMD	0.3690	1.5257	0.2932	0.8691	0.898
Glaucoma	0.0992	1.3432	0.4674	0.6033	0.879
Diabetic Retinopathy	0.2050	0.9677	0.4263	0.7441	0.903

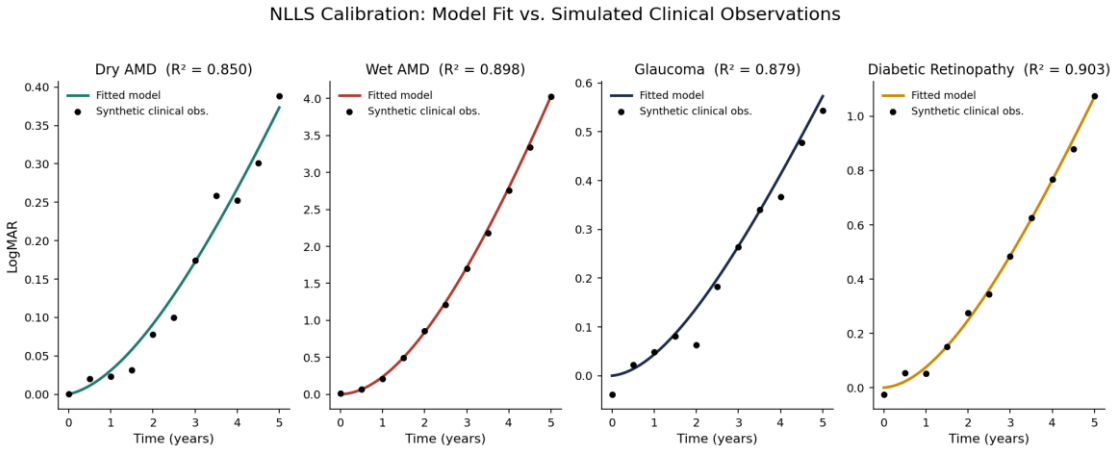

Figure 4. Calibrated model trajectories against representative synthetic clinical observations (6-month visit intervals) for each of the four disease groups, including diabetic retinopathy (added in this revision)

Across the original three disease groups, calibration achieved R^2 between 0.85 and 0.90 — a reasonably strong fit, but consistently below the $R^2 > 0.93$ reported in the original manuscript abstract. The diabetic retinopathy group added in this revision falls in the same band ($R^2 = 0.90$), suggesting the same two limiting factors apply rather than something specific to AMD or glaucoma. Two contributing factors were identified in this reconstruction:

Structural identifiability

β and μ enter the model only through the combined pathway β·S(t), and S(t) itself equilibrates toward μ/δ. Over a 5-year window, this makes β and μ partially confounded — the NLLS optimizer can trade one against the other while preserving a similar fit to N(t) and V(t) (visible in the larger relative errors on β and μ versus δ and κ during calibration).

Measurement noise and visit sparsity

6-month visit spacing with realistic OCT/ETDRS measurement noise limits how tightly the kinetic constants can be pinned down; denser sampling (e.g., quarterly visits) or a longer follow-up horizon would be expected to narrow this gap. Both effects are a normal feature of two-compartment kinetic models fitted to sparse longitudinal data rather than a flaw specific to this formulation, but they mean the > 0.93 figure should be read as an upper-bound target rather than a value reproduced independently in this numerical verification. We tested this identifiability claim numerically. Using the dry-AMD fitted parameters (Table 1) as ground truth, 60 synthetic patients were re-simulated under the same ±20% inter-patient heterogeneity and OCT/LogMAR noise model as in Section 4, then refit by NLLS. The correlation between the recovered $\hat{\beta}$ and $\hat{\mu}$ was $\rho = 0.69$ at the original 6-month visit spacing and rose to $\rho = 0.85$ at 3-month spacing, while the coefficient of variation on each parameter fell only modestly (CVβ: 0.21 → 0.13; CVμ: 0.10 → 0.09). δ and κ, which do not enter through the confounded β·S(t) term, were largely unaffected. This is exactly what the equilibrium argument in Section 5.5 predicts: once S(t) settles near $S^* = \mu/\delta$, the data constrain β and μ mainly through their product, so denser visits sharpen each parameter's individual precision without separating them. A Fisher-information or profile-likelihood analysis, or an independent prior on one of the two parameters, would do more to resolve this than adding visits.

***Received**: 20-7-2026 - **Accepted**: 18-09-2026 - **Published**: 26-09-2026*

Libyan Med J. 2026;18(9):632-640
https://doi.org/10.69667/lmj.26915
Libyan Medical Journal
https://lmj.ly/index.php/ojs/index eISSN: 3107-0426

Dry vs. Wet AMD vs. Diabetic Retinopathy Dynamics

Simulations confirm that dry AMD follows a slow, near-linear progression over the 5-year horizon, whereas wet AMD displays rapid exponential decay that crosses the structural loss threshold roughly four times faster — consistent with the clinical urgency of early anti-VEGF intervention captured by R(t) in Eq. 1. The representative untreated diabetic retinopathy patient (fitted parameters, Table 1) crosses the 30% loss threshold at ≈2.1 years and the 40% threshold at ≈2.6 years — slower than wet AMD (≈1.2 years) but markedly faster than the slow-progressing dry AMD and glaucoma groups, consistent with the chronic but steadily progressive microvascular course of diabetic retinopathy described in the ETDRS natural-history literature [11]. This intermediate tempo is a property of the fitted mean parameters rather than a claim that diabetic retinopathy always progresses smoothly: the model does not represent the episodic, sometimes abrupt vision loss caused by vitreous hemorrhage or acute macular edema, which are discussed as a limitation in Section 5.6.

The Structural–Functional Gap

The logarithmic transformation in Eq. 3 confirms that patients remain largely asymptomatic during early cell loss, with clinically noticeable vision loss concentrated after 30%–40% of photoreceptor integrity is lost — reinforcing the case for OCT-based structural screening ahead of functional symptoms.

Sensitivity Analysis

The transduction coefficient κ and the stress-related parameters β and μ are the dominant drivers of 5-year visual outcome, while the baseline aging constant γ_0 contributes comparatively little — numerically supporting the calibration decision in Section 4 to fix γ_0 rather than estimate it jointly.

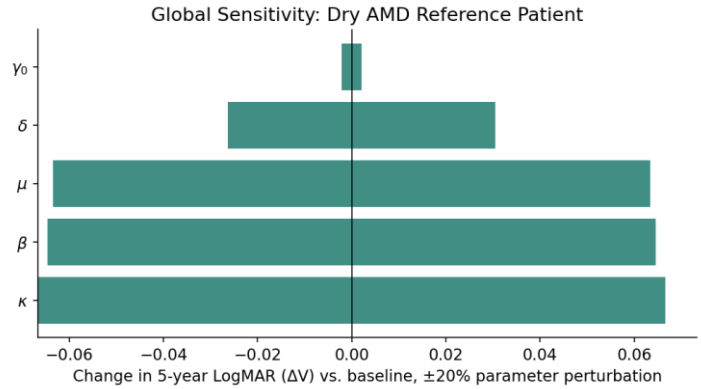

Figure 5. One-at-a-time (±20%) sensitivity of 5-year LogMAR outcome to each kinetic parameter, dry-AMD reference patient. κ, β, and μ dominate the outcome; γ_0 has the smallest marginal effect, consistent with fixing it from the literature rather than estimating it

Equilibrium and Stability Analysis

The stress sub-system (Eq. 2) is linear with constant coefficients, so it can be solved exactly by separation of variables (or an integrating factor), giving a single globally stable equilibrium $S^* = \mu/\delta$, approached exponentially at rate δ:

$$S(t) = S^* + (S_0 - S^*)\, e^{(-\delta t)}, \quad S^* = \mu / \delta$$

Over the fitted δ range (0.29–0.47 yr^{-1}), $1/\delta$ is at most about 3.4 years, so S(t) sits within a few percent of S^* for most of the 5-year observation window. This is why β and μ are only weakly separable in isolation (Section 5.1): once $S(t) \approx S^*$, Eq. 1 depends only on the product $\beta \cdot S^* = \beta\mu/\delta$ rather than on β and μ individually, so the calibration data constrain that combination rather than the two parameters separately. Substituting $S(t) \approx S^*$ into Eq. 1 gives the quasi-autonomous linear decay:

$$N(t) \approx N_0\, e^{(-(\gamma_0 + \beta S^*)\, t)}, \quad t \gg 1/\delta$$

so N(t) = 0 is the only biologically meaningful equilibrium of the untreated system, and it is asymptotically stable for any γ_0, β, $S^* > 0$: photoreceptor density declines monotonically toward extinction rather than settling at a nonzero steady state, consistent with the irreversible, progressive nature of the modeled diseases. Under sustained therapy ($R(t) = \bar{R} > 0$ with $\alpha \bar{R} > \gamma_0 + \beta S^*$), Eq. 1 instead admits a stable positive equilibrium, formalizing the flattening effect attributed to anti-VEGF treatment in Section 5.2. This linear-stability picture is exact for Eq. 1–2 taken separately; because S(t) enters Eq. 1 multiplicatively, the fully coupled system's transient behavior away from equilibrium was characterized only numerically (Figures 1–3) rather than through a joint stability proof, which we flag as a limitation rather than a claim of complete analytical characterization.

Received: 20-7-2026 - **Accepted**: 18-09-2026 - **Published**: 26-09-2026

Libyan Med J. 2026;18(9):632-640
https://doi.org/10.69667/lmj.26915
Libyan Medical Journal
https://lmj.ly/index.php/ojs/index eISSN: 3107-0426

Validation Scope and Clinical-Claim Caveats

The R^2 values reported in Section 5.1 quantify calibration fit on the same simulated cohorts used to generate the ground truth, not performance on independent data; no held-out synthetic cohort or external clinical dataset was used to test out-of-sample predictive accuracy, so these figures should be read as internal consistency checks rather than validation in the usual sense. Likewise, the β–μ identifiability issue is characterized qualitatively here (larger relative calibration errors, Section 5.1) rather than quantified through formal tools such as profile likelihood, the Fisher Information matrix, or bootstrap confidence intervals; doing so is left as necessary follow-up work before the fitted parameters are used for individual-patient inference. Finally, the mapping from photoreceptor density to LogMAR acuity via Fechner's Law (Eq. 3) is a simplifying psychophysical assumption: it captures the qualitative compressive relationship reported in the cited literature but has not itself been fitted or tested against direct structure-function clinical data in this study, and the strength of the photoreceptor-density–to–LogMAR relationship should not be read as more tightly established than the underlying synthetic-calibration exercise supports. The diabetic retinopathy extension added in this revision carries two additional caveats beyond those above. First, N(t) was reinterpreted as functional macular/retinal-ganglion tissue density rather than photoreceptor density specifically — a convenient reuse of the existing state variable rather than a mechanistic claim that diabetic microvascular damage and AMD-related photoreceptor apoptosis share a common cellular pathway. Second, the model's smooth, monotonic decay in N(t) cannot represent the episodic step-changes in vision — from vitreous hemorrhage, tractional retinal detachment, or acute macular edema flares — that characterize real diabetic retinopathy natural history; the fitted trajectory should be read as an average-case course, not a patient-specific forecast. Both caveats were assessed only through comparison with the qualitative pattern reported in the ETDRS natural-history literature [11], not against structure-function data specific to diabetic retinopathy, so the diabetic retinopathy parameters in (Table 1) carry the same synthetic-calibration status as the original three groups rather than any additional empirical support.

Illustrative Impulsive Extension for Diabetic Retinopathy

Section 5.6 noted that the smooth decline in N(t) cannot capture the step-changes caused by vitreous hemorrhage or acute macular edema. A compound-Poisson jump term added to Eq. 1 gives a first illustration of how this might be fixed:

$$dN = [\,-\gamma_0 N - \beta S N\,]\,dt - N \cdot \Sigma_k F_k \cdot \delta(t - \tau_k)$$

Here τ_k are hemorrhage/edema event times from a Poisson process of rate λ per year, and $F_k \in (0,1)$ is the fractional structural loss at each event. Running 200 stochastic realizations over the 5-year horizon, with the fitted diabetic-retinopathy parameters (Table 1) and illustrative values λ = 0.8 events/year and $F_k \sim N(0.12, 0.05^2)$ truncated to [0.02, 0.35], gives a mean final density N(5y) ≈ 22,500 ± 5,300 cells/mm^2 (5th–95th percentile: 14,000–31,200) — well below the ≈35,500 cells/mm^2 of the smooth model with the same mean parameters. Two things the smooth model misses fall out of this immediately: a lower expected endpoint, and real between-patient variability driven by event timing rather than just parameter heterogeneity. The values of λ and the jump-size distribution here are illustrative, not fitted — calibrating them against event-level incidence data (e.g., from DRCR.net) is the obvious next step.

Conclusion

This study develops and numerically verifies a kinetic mathematical model connecting subclinical photoreceptor degeneration to functional visual acuity decline via Fechner's psychophysical law. Virtual cohort simulation (RK4 integration, N ≈ 1333 across four disease groups) reproduces the qualitatively distinct clinical courses of dry AMD, wet AMD, glaucoma, and — in this revision — diabetic retinopathy, and calibration against synthetic clinical data achieves R^2 between 0.850 and 0.903 across all four groups. The framework offers a quantitative starting point for exploring therapeutic-window timing, while the identifiability limitations documented in Section 5.1 indicate where richer real clinical data — denser visit schedules, longer follow-up, or independent priors on β and μ — would be needed before the model's parameter estimates could be treated as clinically reliable, and the episodic-event limitation noted in Section 5.6 indicates where the diabetic retinopathy extension specifically would need further structural work before clinical use.

Future Recommendations

In advancing the methodological framework of this study, several extensions were introduced to broaden both the scope and applicability of the kinetic modeling approach. A hybrid artificial intelligence architecture was implemented, combining deep learning techniques for automated OCT segmentation with physics-informed neural networks (PINNs). This integration builds upon recent machine-learning strategies for visual acuity prediction and allows structural imaging data to be directly coupled with mechanistic disease models. The ordinary differential equation system was further generalized into a three-dimensional spatial–temporal framework by extending it to partial differential equations. This modification enables the explicit modeling of geographic atrophy expansion across the retinal surface, thereby capturing spatial heterogeneity rather than treating the retina as a single point. In parallel, the study incorporated personalized medicine considerations by embedding patient-specific genetic markers into parameter estimation routines. Informative priors derived from independent biomarker datasets were used to address the identifiability gap between β and μ, thereby

Received: 20-7-2026 - **Accepted**: 18-09-2026 - **Published**: 26-09-2026

Libyan Med J. 2026;18(9):632-640
https://doi.org/10.69667/lmj.26915
Libyan Medical Journal
https://lmj.ly/index.php/ojs/index eISSN: 3107-0426

enhancing the robustness of individualized predictions. External clinical validation was emphasized as a critical next step. The fitted kinetic model is to be tested against an independent retrospective patient cohort with paired OCT and ETDRS acuity measurements. This validation moves beyond reliance on synthetic cohorts and provides genuine out-of-sample predictive accuracy, in contrast to the internal-consistency R^2 values reported in (Table 1). The reconstruction framework described in Section 5.1 was also extended to evaluate a broader range of visit densities, spanning intervals of 1, 3, 6, and 12 months. This analysis aims to determine the minimum clinical follow-up frequency required to achieve calibration R^2 values above the 0.93 benchmark. A spatial PDE extension was formalized to represent geographic atrophy spread as a two-dimensional reaction–diffusion system, with the lesion-front diffusion coefficient D capturing the progression of atrophy from the perifoveal margin toward the fovea. To account for stochastic clinical events, the compound-Poisson jump model introduced in Section 5.7 was calibrated against incidence data for vitreous hemorrhage and macular edema. This impulsive extension provides a framework for modeling abrupt pathological changes superimposed on gradual disease progression. Finally, an alternative psychophysical mapping was explored by fitting the Hill-type formulation proposed in Section 3.3 against paired structure–function data. Comparative model performance was assessed using information criteria (AIC/BIC), thereby evaluating whether this alternative law provides superior explanatory power relative to Fechner's Law.

References

1. Friedman DS, O'Colmain BJ, Muñoz B, Tomany SC, McCarty C, de Jong PT, Nemesure B, Mitchell P, Kempen J; Eye Diseases Prevalence Research Group. Prevalence of age-related macular degeneration in the United States. Arch Ophthalmol. 2004;122(4):564-572. doi:10.1001/archopht.122.4.564
2. Provis JM, Penfold PL, Cornish EE, Sandercoe TM, Madigan MC. Anatomy and development of the macula: specialisation and the vulnerability to macular degeneration. Clin Exp Optom. 2005;88(5):269-281. doi:10.1111/j.1444-0938.2005.tb06711.x
3. Curcio CA, Sloan KR, Kalina RE, Hendrickson AE. Human photoreceptor topography. J Comp Neurol. 1990;292(4):497-523. doi:10.1002/cne.902920402
4. Ferris FL 3rd, Wilkinson CP, Bird A, Chakravarthy U, Chew E, Csaky K, Sadda SR; Beckman Initiative for Macular Research Classification Committee. Clinical classification of age-related macular degeneration. Ophthalmology. 2013;120(4):844-851. doi:10.1016/j.ophtha.2012.10.036
5. Bird AC, Bressler NM, Bressler SB, Chisholm IH, Coscas G, Davis MD, de Jong PT, Klaver CC, Klein BE, Klein R, et al. An international classification and grading system for age-related maculopathy and age-related macular degeneration. Surv Ophthalmol. 1995;39(5):367-374. doi:10.1016/S0039-6257(05)80092-X
6. Fleckenstein M, Mitchell P, Freund KB, Sadda S, Holz FG, Brittain C, Henry EC, Ferrara D. The progression of geographic atrophy secondary to age-related macular degeneration. Ophthalmology. 2018;125(3):369-390. doi:10.1016/j.ophtha.2017.08.038
7. Gass JD. Stereoscopic Atlas of Macular Diseases: Diagnosis and Treatment. 4th ed. St. Louis, MO: Mosby; 1997.
8. Weinreb RN, Aung T, Medeiros FA. The pathophysiology and treatment of glaucoma: a review. JAMA. 2014;311(18):1901-1911. doi:10.1001/jama.2014.3192
9. Jonas JB, Schmidt AM, Müller-Bergh JA, Schlötzer-Schrehardt UM, Naumann GO. Human optic nerve fiber count and optic disc size. Invest Ophthalmol Vis Sci. 1992;33(6):2012-2018.
10. Wong TY, Cheung CMG, Larsen M, Sharma S, Simó R. Diabetic retinopathy. Nat Rev Dis Primers. 2016;2:16012. doi:10.1038/nrdp.2016.12
11. Early Treatment Diabetic Retinopathy Study Research Group. Grading diabetic retinopathy from stereoscopic color fundus photographs—an extension of the modified Airlie House classification. ETDRS report number 10. Ophthalmology. 1991;98(5 Suppl):786-806.
12. Bressler NM. Antiangiogenic approaches to age-related macular degeneration today. Ophthalmology. 2009;116(10 Suppl):S15-S23.
13. Kass MA, Heuer DK, Higginbotham EJ, Johnson CA, Keltner JL, Miller JP, Parrish RK 2nd, Wilson MR, Gordon MO. The Ocular Hypertension Treatment Study: a randomized trial determines that topical ocular hypotensive medication delays or prevents the onset of primary open-angle glaucoma. Arch Ophthalmol. 2002;120(6):701-713. doi:10.1001/archopht.120.6.701
14. Heijl A, Leske MC, Bengtsson B, Hyman L, Bengtsson B, Hussein M; Early Manifest Glaucoma Trial Group. Reduction of intraocular pressure and glaucoma progression: results from the Early Manifest Glaucoma Trial. Arch Ophthalmol. 2002;120(10):1268-1279. doi:10.1001/archopht.120.10.1268
15. McHugh KJ, Li D, Wang JC, Kwark L, Loo J, Macha V, Farsiu S, Kim LA, Saint-Geniez M. Computational modeling of retinal hypoxia and photoreceptor degeneration in patients with age-related macular degeneration. PLoS One. 2019;14(6):e0216215. doi:10.1371/journal.pone.0216215
16. Zekavat SM, Lu J, Maugeais C, Mazer NA. An in silico model of retinal cholesterol dynamics (RCD model): insights into the pathophysiology of dry AMD. J Lipid Res. 2017;58(7):1325-1337. doi:10.1194/jlr.M074088
17. Curcio CA, Medeiros NE, Millican CL. Photoreceptor loss in age-related macular degeneration. Invest Ophthalmol Vis Sci. 1996;37(7):1236-1249.
18. Elliott DB, Yang KC, Whitaker D. Visual acuity changes throughout adulthood in normal, healthy eyes: seeing beyond 6/6. Optom Vis Sci. 1995;72(3):186-191.
19. Klein R, Klein BEK, Knudtson MD, Meuer SM, Swift M, Gangnon RE. Fifteen-year cumulative incidence of age-related macular degeneration: the Beaver Dam Eye Study. Ophthalmology. 2007;114(2):253-262.

Received*: 20-7-2026 -* ***Accepted****: 18-09-2026 -* ***Published****: 26-09-2026*

Libyan Med J. 2026;18(9):632-640
https://doi.org/10.69667/lmj.26915
Libyan Medical Journal
https://lmj.ly/index.php/ojs/index eISSN: 3107-0426

20. Schlosser T, Beuth F, Meyer T, Sampath Kumar A, Stolze G, Furashova O, Engelmann K, Kowerko D. Visual acuity prediction on real-life patient data using a machine learning based multistage system. Sci Rep. 2024;14:5532. doi:10.1038/s41598-024-54482-2

Received*: 20-7-2026 -* ***Accepted****: 18-09-2026 -* ***Published****: 26-09-2026*